Chapter 14

# Application of Aligned Carbon Nanotube-Reinforced Polymer Composite to Electrothermal Actuator

Keiichi Shirasu, Go Yamamoto and Toshiyuki Hashida

Additional information is available at the end of the chapter

http://dx.doi.org/10.5772/62509

**Abstract**

Electrothermal bimorph actuators have been widely researched, comprising two layers with asymmetric expansion that generate a bending displacement. Actuation performance greatly relies upon the difference of the coefficients of thermal expansion (CTE) between the two material layers. Since traditionally used bimorph materials have positive CTE values, the generated displacements are restricted because of their relatively low CTE difference. Currently, the synthesis and characterization of carbon nanotube (CNT)/polymer composite actuators are topics of intense research activity. CNTs have been attracting much interest because of their superior electrical, thermal and mechanical properties. In addition, the negative CTE value of CNTs in the axial direction has been investigated analytically, leading one to expect that the CTE of the composites in a direction parallel to the CNT alignment will drastically decrease by containing the aligned CNTs into polymer materials. In this chapter, an experimental method for determining the CTE of a CNT in the axial direction is discussed. Based on this result, we demonstrate an electrothermal bimorph actuator having a large bending displacement and high force output using an aligned CNT-reinforced epoxy composite and thin aluminum foil. Performance characteristics including power and work output per unit volume versus frequency are also reviewed.

**Keywords:** Carbon nanotube, Composite, Young's modulus, Coefficient of thermal expansion, Actuator

## 1. Introduction

Electrothermal actuators, which have a displacement/force output at low-voltage operation conditions and a simple fabrication process, are good for applications such as precise-tracking positioning devices, artificial muscles and manipulators [1–3]. One of the electrothermal actuation schemes is the so-called bimorph effect [4], where two materials with different thermal expansions are combined in a bimorph cantilever. The thermal expansion mismatch between the two layers of the cantilever can produce a bending displacement when current is passed through the component. Traditionally used bimorph materials include metals, metal oxides and silicon [1, 5–7], most of which have a positive coefficient of thermal expansion (CTE). Therefore, the generated displacements of these bimorph materials are restricted because of the relatively low CTE difference between them.

Currently, the synthesis and characterization of carbon nanotube (CNT)/polymer composite actuators are topics of intense research activity [8–10]. CNTs have been attracting much interest because of their potential applications as a next-generation electronic material. In particular, their superior electrical, thermal and mechanical properties, including high electrical and thermal conductivity [11, 12] and extremely high mechanical strength exceeding 100 GPa [13], make them a candidate material for nano- and microscale actuators, composites and electronic devices. In addition, the negative CTE of CNTs in the axial direction has been investigated analytically [14–17], and is found to be much lower than that of polymer materials. Thus, it is expected that the CTE of the composites in the direction parallel to CNT alignment will drastically decrease with the addition of aligned CNTs into the polymer material. However, there is no experimental study on the axial CTE of CNTs. Therefore, for such applications, knowledge of the CTE of CNTs is crucial.

Recently, Zhang et al. [18]have developed continuous multiwalled CNT (MWCNT) sheets by directly drawing MWCNTs from super-aligned MWCNT arrays. The MWCNT sheet fabrication technology has allowed aligned MWCNT-reinforced polymer composites to be prepared, where the resultant composites possess a high MWCNT volume fraction and achieve a high Young's modulus [19–23]. In addition, because these kind of MWCNTs have high aspect ratios and are well-aligned in the composites, it can be expected that an evaluation of the CTE of the composites in the MWCNT alignment direction makes it possible to evaluate the axial CTE of the MWCNTs.

In this chapter, to determine the axial CTE of MWCNTs, the CTE of aligned MWCNT-reinforced epoxy composites in the MWCNT alignment direction is measured and the axial CTE of the MWCNTs is estimated using the rule of mixtures. We have found that the MWCNTs in the axial direction possess a negative CTE, and that the CTE of the composites in the MWCNT alignment direction became negative with the addition of more than 10 vol.% MWCNTs. Based on this result, we demonstrate an electrothermal bimorph actuator with a large bending displacement and a high force output by using an aligned MWCNT-reinforced epoxy composite and thin aluminum foil. Because the thermal expansion mismatch between the composite layer and the aluminum layer is enormous, the same temperature rise leads to a larger bending actuation of the structure compared with the conventional electrothermal

http://dx.doi.org/10.5772/62509

bimorph actuators. Furthermore, because the Young's modulus of the composite is expected to be enhanced by including aligned MWCNTs in the polymer matrix as mentioned above, the force output of the actuator comprising the composite is also expected to increase.

## 2. Experimental procedure

### 2.1. Sample preparation

The MWCNTs were grown vertically on an oxidized silicon wafer substrate with chemical vapor deposition using $C_2H_2$ and $FeCl_2$ as the base material and the catalyst, respectively. Hereafter, the vertically aligned MWCNTs grown on a substrate are referred to as MWCNT arrays. The detailed procedure for the fabrication of MWCNT arrays has been reported elsewhere [24]. The average diameter and length of the MWCNTs were 39 nm (15–57 nm) and >600 μm, respectively. The MWCNT monolithic sheets were drawn out of the MWCNT arrays and wound onto a rotating plate (**Figure 1a**). In this study, five kinds of stacked MWCNT monolithic sheets (50–250 layers) were prepared.

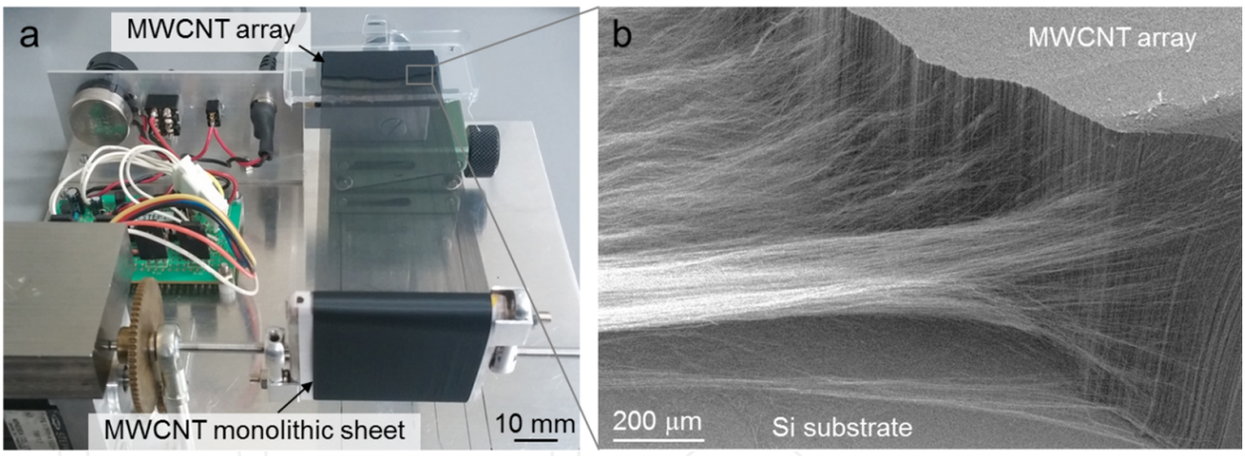


**Figure 1.** (a) Photograph and (b) SEM image of a MWCNT array and aligned MWCNT sheet.

Aligned MWCNT/epoxy composites were prepared by a hot-melt prepreg method [21], wherein the MWCNT monolithic sheet was pre-impregnated with an epoxy matrix. A partially cured epoxy resin (B-stage epoxy) with a release paper was used as the starting materials, where the epoxy resin comprised bisphenol-A type epoxy, novolac-type epoxy and an aromatic diamine curing agent. A stacked MWCNT monolithic sheet about 20 mm wide and about 45 mm in length was placed on a polytetrafluoroethylene sheet and covered with the epoxy resin film with the release paper. The epoxy resin was then impregnated into the MWCNT monolithic sheet at 90°C for 3 min between the steel plates of the hot press (AS ONE AH-4015, Japan). After peeling off the release paper from the MWCNT sheet now impregnated with the epoxy resin (prepreg sheet), the prepreg sheet was cured at 130°C for 1.5 h at the

pressure of 1 MPa using the hot press, forming a film specimen. To evaluate the actuator properties, an aligned MWCNT-reinforced epoxy composite/aluminum laminate was prepared. The prepreg sheet was prepared under the same processing condition as mentioned above. Subsequently, after peeling off the release paper from the prepreg sheet, aluminum foil was stacked on the prepreg sheet and cured at 130°C for 1.5 h at the pressure of 1 MPa using the hot press.

### 2.2. Evaluation of mechanical properties and CTE

Tensile tests of the aligned MWCNT/epoxy composites were performed using a tensile test apparatus (Instron Model 5965, USA) with a 50 N load cell. Strain was measured by a laser displacement meter (Keyence LS-7600, Japan) with a resolution of 0.1 μm, whereupon the Young's modulus was calculated from the slope of the stress-strain curve. The thickness and width dimensions of the tensile testing samples were measured by a scanning electron microscope (SEM). The gage length was about 18 mm and the testing speed was 0.2 mm/min, and at least three samples were tested from each batch of composites. Uniaxial tensile tests of individual MWCNT were carried out with a manipulator inside the vacuum chamber of the SEM [25, 26]. Further details of the experimental procedure are described elsewhere [26]. In this study, the diameter of the individual MWCNTs was measured from transmission electron microscope (TEM) images, wherein 23 MWCNTs were observed and measured. The in-plane MWCNT alignment distribution for the composites was observed using an SEM (JEOL JSM6510, Japan) and a TEM (JEOL JEM-2100F, Japan). A thin sample for TEM observations was prepared using a focused ion beam milling machine (Hitachi FB2200, Japan), with a machined area that was approximately 20 μm wide, 4 μm deep and 0.3 μm thick.

We measured the CTE of the aligned MWCNT/epoxy composite films using the experimental setup schematically shown in **Figure 2**. The dimensions of the composite film sample were 19 × 2 × 0.019 – 0.030 $mm^3$ (length × width × thickness), where the length is along the direction parallel to the MWCNT alignment. The sample was placed on a hot plate and the temperature measured by a thermocouple placed in contact with the composite sample. The length change was then measured by the laser displacement meter in the temperature range 30–60°C and with a heating rate in the range of 1.8–79.0 K/min. In this study, we evaluated the average CTE of the composites in the above-mentioned temperature range. The formula for the CTE of the composites, $\alpha_c$, was given by

$$\alpha_c = \frac{\Delta L/L}{\Delta T}, \tag{1}$$

where $L$ is the initial length, $\Delta L$ is the change in length and $\Delta T$ is the change in temperature (30 K) of the composite sample. The slope of the curve $\Delta L/L$ vs. $\Delta T$ over the temperature range was obtained using experimental data to determine $\alpha_c$.

http://dx.doi.org/10.5772/62509

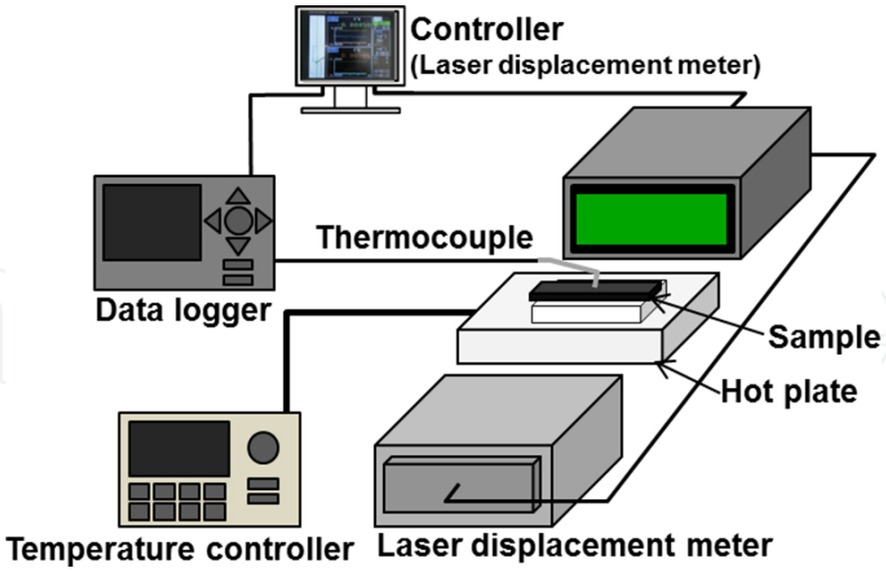


**Figure 2.** Schematic illustration of experimental setup for determining the CTE of MWCNT/epoxy composites.

### 2.3. Evaluation of actuator properties

The experimental setup used to characterize the actuator performance is shown in **Figure 3**. To evaluate the actuator property, an electrothermal actuator was prepared using the composite/aluminum laminate, where the MWCNT volume fraction in the composite layer was 27 vol.%. As shown in **Figure 3**a, a U-shaped actuator was formed by cutting out the middle part of the composite/aluminum laminate, where the CNT-aligned direction is parallel to the length direction of the U-shaped actuator. The dimension of the entire U-shaped actuator was 20 × 5 × 0.038 $mm^3$ (length × width × thickness), wherein the width of each beam was around 2 mm. A gold coating was sputtered onto the surface of the composite layer to decrease the contact resistance between the composite layer and the copper electrodes and to enhance the conductivity in the composite layer. The edge of the sample was masked during deposition by a polyimide tape to prevent electrical shorting on the sidewalls of the sample by the gold layer. The top end of the sample was sandwiched between glass plates and the composite layer was then attached to two copper electrodes. The free length of the actuator was 16 mm. The sample was suspended vertically in a glove box chamber and a DC voltage was applied using a power supply (KEITHLEY 2400, USA). The square waveform input voltage on the composite layer was controlled using a Labview program, and the bending of the sample was captured by the laser displacement meter. The sample surface temperature during actuation was measured using infrared thermography (Apiste FSV-1200, Japan), where the temperature data were obtained from the bare surface of the composite layer. Calibration of the thermography was performed by also heating the sample on a hot plate and using a thermocouple placed on the composite layer to measure the sample temperature. The emissivity of the composite was determined based on the thermocouple temperature measurements. The temperature, displacement and applied voltage values were automatically recorded every 200 ms to a text file using data logger (Graphtec GL220, Japan).

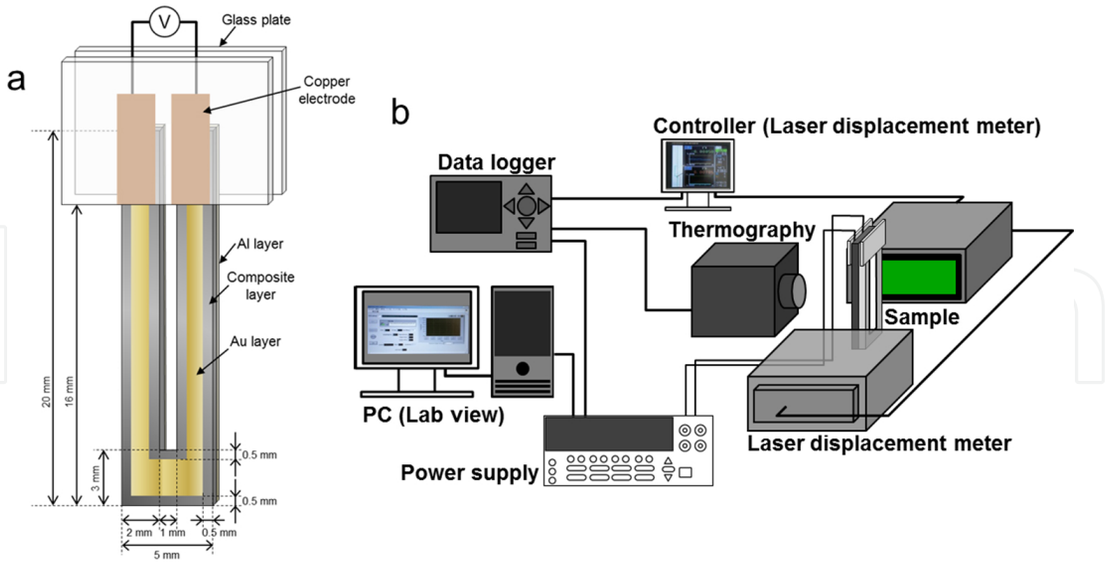


**Figure 3.** Schematic illustration of (a) the U-shaped actuator and (b) experimental setup for determining bending displacement of the U-shaped actuator.

## 3. Results and discussion

### 3.1. Mechanical properties

A MWCNT array prepared in this study is shown in **Figure 1**b. Because of their high areal density and the strong interaction between MWCNTs, well-aligned MWCNT monolithic sheets are produced easily from the MWCNT array by pulling [24]. To evaluate the Young's modulus of individual MWCNTs, uniaxial tensile tests of single MWCNTs were carried out using a nanomanipulator system. The Young's modulus averaged from the values obtained from 23 MWCNTs was 210 GPa.

A SEM image of the MWCNT distribution in the composite is shown in **Figure 4**a. The majority of the MWCNTs are aligned, although some MWCNTs are inclined with respect to the alignment direction. A TEM image shown in **Figure 4**b shows the morphology of the internal structure of the composites, where it is seen that the epoxy resin penetrates thoroughly between the MWCNTs. The TEM image indicates that the densely aligned MWCNT composites are successfully fabricated using the present processing method with only a limited amount of pores, which are marked by black arrows (**Figure 4**b).

The dependence of the Young's modulus of the composites upon the MWCNT volume fraction is shown in **Figure 5**, where it is seen to increase linearly with the increasing MWCNT volume fraction. The Young's modulus of the composite containing 27 vol.% MWCNTs reaches 56.8 ± 3.9 GPa, which is one order of magnitude higher than that of randomly oriented CNT/polymer composites [27]. In these MWCNT/epoxy composites, the MWCNTs possessed a high aspect ratio (length/diameter >15,000) and were aligned along the same direction. This suggests that the composites prepared in this study can be modeled as continuous fibers aligned in parallel

http://dx.doi.org/10.5772/62509

within the epoxy matrix [28]. Therefore, the Young's modulus of the composites in the direction of the MWCNT alignment, $E_c$, may be expressed using the rule of mixtures [28] such that

$$E_c = (1 - V_f)E_m + V_f E_f, \tag{2}$$

where $E_m$ and $E_f$ are the Young's moduli of the epoxy and the MWCNTs, respectively, and $V_f$ is the MWCNT volume fraction. Using Eq. (2), the Young's modulus of the MWCNTs is calculated to be 200 GPa, which is close to the Young's modulus of the individual MWCNTs measured by the uniaxial tensile tests (210 GPa). The solid line in **Figure 5** is a regression line provided by the least-squares regression analysis (the regression coefficient $R^2$ is calculated to be 0.97). These results suggest that the Young's modulus of the composites in the direction of the MWCNT alignment can be evaluated by the rule of mixtures.

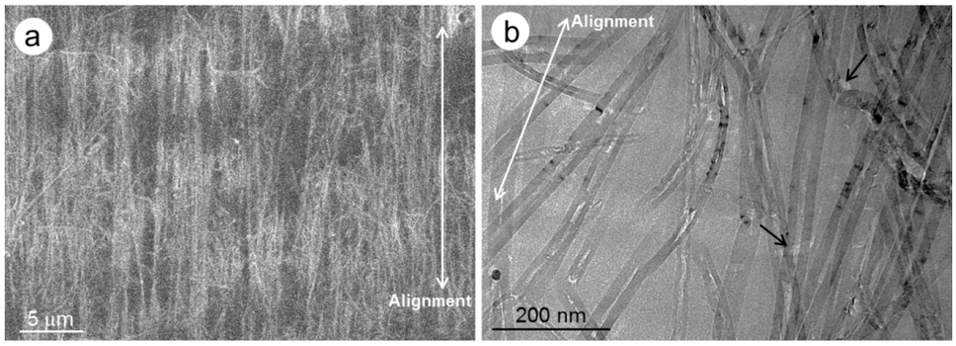


**Figure 4.** Aligned MWCNT/epoxy composites showing in-plane MWCNT distribution acquired by (a) SEM and (b) TEM. The MWCNT volume fraction is (a) 27 and (b) 22 vol.%.

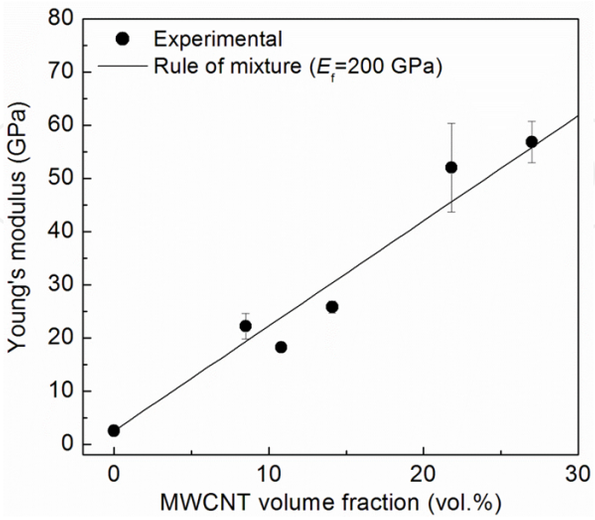


**Figure 5.** Young's modulus of the aligned MWCNT-reinforced epoxy composites as a function of MWCNT volume fraction.

### 3.2. Coefficient of thermal expansion

We evaluate the CTE of the aligned MWCNT/epoxy composites. **Figure 6**a shows the variation of the thermal strain of the composites in the axial direction of the MWCNT alignment and of pure epoxy as a function of temperature change. The thermal strain of the epoxy increases with the increasing temperature, and the CTE of the epoxy is $7.0 \times 10^{-5}$ $K^{-1}$. The CTE dramatically decreases, however, with the addition of 9 vol.% MWCNTs, and thermal contraction can be observed in composites containing more than 11 vol.% MWCNTs. The dependence of the CTE upon the MWCNT volume fraction is shown in **Figure 6**b, where it can be seen that, though some variations are observed, the CTE tends to decrease with the increasing MWCNT volume fraction. Ultimately, the CTE of the composite containing 27 vol.% MWCNTs is $-0.7 \times 10^{-5}$ $K^{-1}$. As mentioned above, the composites prepared in this study can be modeled as continuous fibers aligned in parallel within the epoxy matrix. Thus, the CTE of the composites in the direction of the MWCNT alignment, $\alpha_c$, may be expressed using the rule of mixtures [28] such that

$$\alpha_c = \frac{\alpha_m (1 - V_f) E_m + \alpha_f V_f E_f}{(1 - V_f) E_m + V_f E_f}, \tag{3}$$

where $\alpha_m$ and $\alpha_f$ are the CTEs of the epoxy and MWCNTs, respectively. As mentioned above, the epoxy resin penetrates thoroughly between individual MWCNTs (**Figure 4**b). Thus, it may be reasonable to substitute the Young's modulus of the individual MWCNTs for $E_f$ in the rule of mixtures. Substituting $E_m$ = 2.5 GPa, $E_f$ = 210 GPa and $\alpha_m = 7.0 \times 10^{-5}$ $K^{-1}$ into Eq. (3) and performing the least square regression analyses for the data shown in **Figure 6**b, the value of $\alpha_f$ is calculated to be $-1.1 \times 10^{-5}$ $K^{-1}$. The solid line in **Figure 6**b is a regression line provided by the least-squares regression analysis (the regression coefficient $R^2$ is calculated to be 0.98).

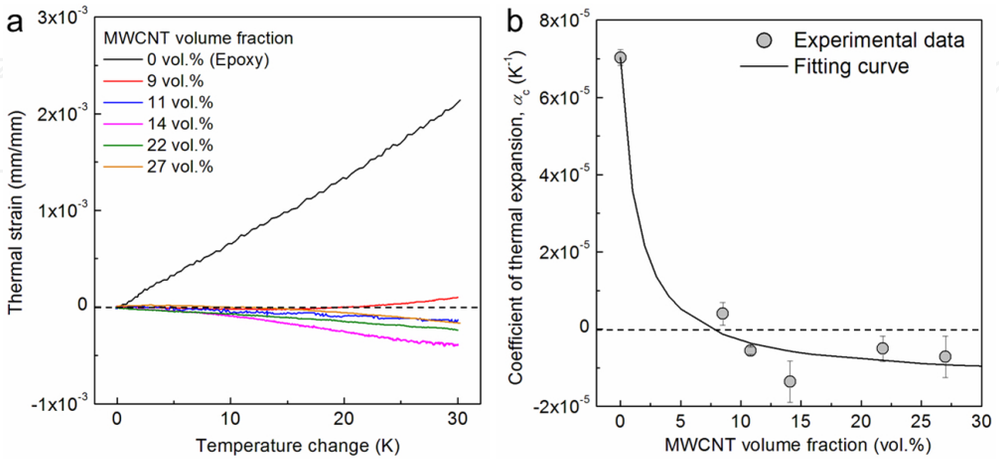


**Figure 6.** (a) Thermal strain of composites as a function of the temperature change. (b) Coefficient of thermal expansion of the composites as a function of the MWCNT volume fraction.

http://dx.doi.org/10.5772/62509

Some numerical and theoretical studies have been performed on the CTE in the axial direction of the CNTs. The axial CTE values of single-walled CNTs (SWCNTs) and MWCNTs reported in previous studies [14–17, 29, 30] are summarized in **Table 1**, where the majority of the previous studies have predicted that the CNTs contract axially below the temperature of 400 K. The thermal expansion of solids is well understood in terms of Grüneisen theory [31], and whether a solid expands or contracts upon heating depends upon the balance between phonon modes with positive and negative Grüneisen parameters. At low temperatures, transverse acoustic modes that correspond to the out-of-plane atomic vibrations of the crystal lattice may exhibit negative Grüneisen parameters. Schelling et al. [14] have reported that the CTE in the axial direction for SWCNTs is $-0.9 \times 10^{-6}$ $K^{-1}$ at room temperature, and this fact is associated with the negative Grüneisen parameters. The axial CTE value of the MWCNTs measured in this study is in reasonable agreement with those of the CNTs reported previously [14–17].

| Material | CTE ($K^{-1}$) | Temperature (K) | Method | Ref. |
|---|---|---|---|---|
| (10,10) SWCNT | $-0.9 \times 10^{-6}$ | RT | Theory | 14 |
| (10,10) SWCNT | $2.5 \times 10^{-6}$ | High | Theory | 14 |
| (10,10) SWCNT | $-1.2 \times 10^{-5}$ | 400 | Simulation | 15 |
| (5,5) SWCNT | $-0.2 - 3.6 \times 10^{-6}$ | 250–1600 | Theory | 16 |
| (9,0) SWCNT | $-0.4 - 3.3 \times 10^{-6}$ | 250–1600 | Theory | 16 |
| (100,100) SWCNT | $-1.6 \times 10^{-5}$ | 300 | Simulation | 17 |
| MWCNT | $0 - -1.0 \times 10^{-6}$ | 300 | Simulation | 17 |
| (5,5) SWCNT | $3.9 \times 10^{-6}$ | 300–800 | Simulation | 29 |
| (10,10) SWCNT | $2.4 \times 10^{-6}$ | 300–800 | Simulation | 29 |
| (10,10) SWCNT | $0–2.1 \times 10^{-6}$ | 0–2000 | Simulation | 30 |

**Table 1.** Full list of the axial CTE of CNTs. Shown are the CNT type, axial CTE of the CNTs, temperature range and method.

### 3.3. Actuator properties

The cross-sectional view of the laminate comprising the composite containing 27 vol.% MWCNTs and aluminum thin foil is shown in **Figure 7**. The SEM image indicates that the two layers are tightly bonded to each other using the present processing method without delamination in the laminate. The composite layer and aluminum layer have thicknesses of about 30 and 8 μm, respectively. We now evaluate the bending actuation of the U-shaped actuator. **Figure 8** shows the bending actuation performance and temperature variation of the U-shaped actuator. When a DC voltage of 3.0 V was applied, the actuator began to bend immediately and the free-end displacement of the actuator reached 3.0 mm. The free end returned to its initial position after the power source was cut off. The bending displacement was almost identical to the temperature variation during the actuation process.

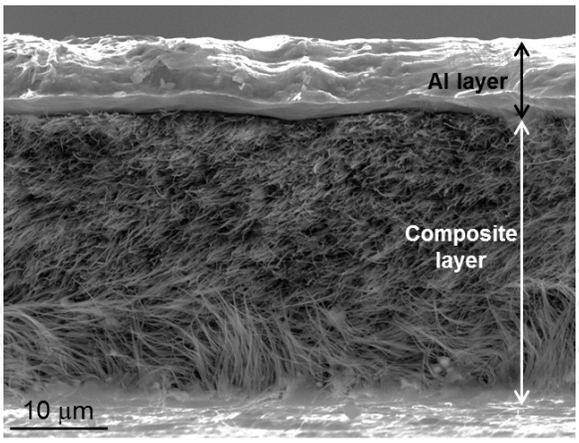


**Figure 7.** SEM image showing the cross-section of the composite/aluminum laminate.

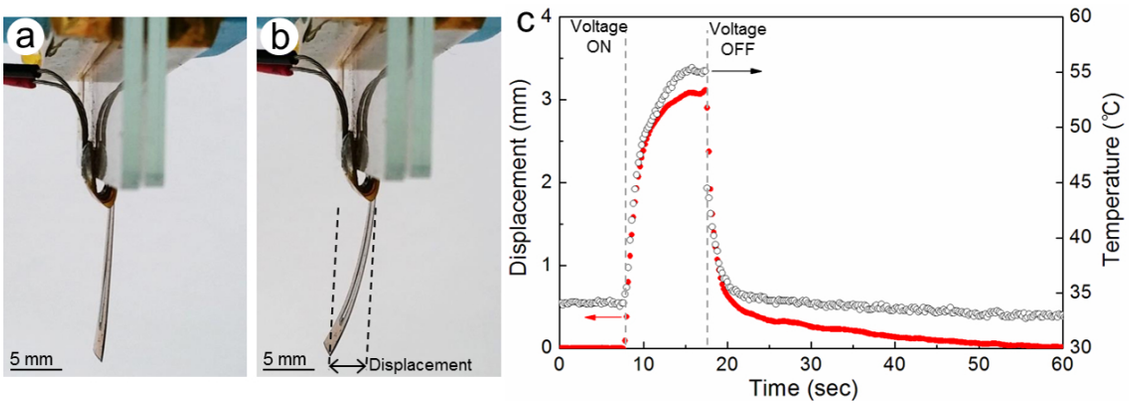


**Figure 8.** Photographs of an actuator (a) without and (b) with an applied DC voltage of 3.0 V. (c) Bending displacement and temperature variation of the actuator with an applied DC voltage of 3.0 V.

The dependences of the displacement upon the applied voltage and temperature are shown in **Figure 9**a and b. The glass transition temperature of the epoxy used in this study was 130°C, so we evaluated the bending displacement of the actuator at a temperature range of 30–120°C, below the glass transition temperature. The bending displacement is proportional to the temperature change and to the square of the applied voltage, and reaches 7.6 mm under a DC voltage of 5.2 V, which suggests that the actuation mechanism is owing to the Joule heating. The CTE of the composite in the MWCNT alignment direction has been measured to be −0.7 × $10^{-6}$ $K^{-1}$ (**Figure 6**). Thus, upon applying an electric voltage on the actuator, the composite layer is directly heated and shrinks along its length. The aluminum layer, however, is heated up by the heat that diffuses from the composite layer and results in a thermal expansion. The vast thermal expansion mismatch between the composite layer and the aluminum layer is expected to cause a large bending displacement for the actuator under electric stimulation. The temperature dependence of the force output is shown in **Figure 9**c. The force output, *F*, is calculated by the following equation while assuming that the bending displacement is equal to that of a cantilever model subject to a tip concentrated load:

http://dx.doi.org/10.5772/62509

$$F = \frac{3\delta(E_1 I_1 + E_2 I_2)}{L^3}, \tag{4}$$

where $\delta$ is the bending displacement, $E$ is the Young's modulus, $I$ is the second moment of inertia and $L$ is the length of the actuator. The subscripts 1 and 2 for $E$ and $I$ refer to the composite layer and aluminum layer, respectively. **Figure 9**c shows that the force output is nearly in line with the temperature change, and reaches 9.0 mN at 5.2 V. **Figure 10** shows the vibration amplitude and calculated force output of the actuator at the square wave voltage with different frequencies. With an increasing frequency higher than 0.25 Hz, both the vibration amplitude and the force output gradually decrease. According to the thermal actuation mechanism, the maximal vibration frequency of the actuator is determined by its heat generation and dissipation rate. For the electrical-induced thermal actuator, the heating and cooling rate will lag the rate of the current charge at a frequency higher than 0.25 Hz, which leads to the decrease of the vibration amplitude and force output.

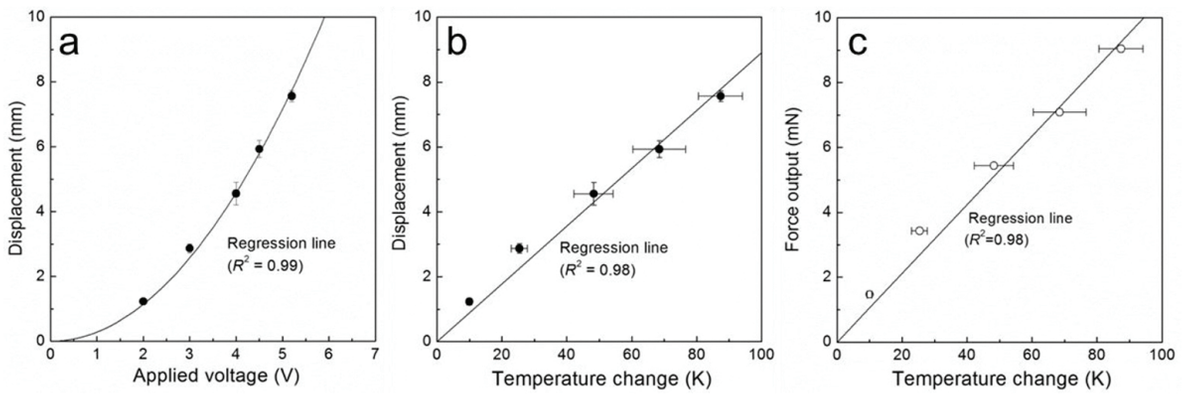


**Figure 9.** Bending displacement of the actuator as functions of (a) applied voltage and (b) temperature change. (c) Calculated force output as a function of temperature change.

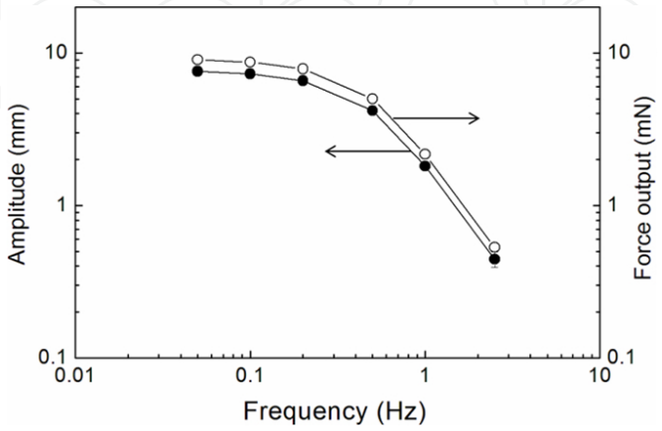


**Figure 10.** Vibration amplitude and force output as a function of frequency of the applied 5.2 V square voltage.

Where an actuator must operate cyclically, considerations of frequency and power become relevant. The maximum power output per unit volume, $P_{max}$, is defined by

$$P_{max} = W_{max} \Big/ \frac{t}{2} = 2fW_{max}, \tag{5}$$

where $t$ is the period of time, $f$ is the frequency and $W_{max}$ is the maximum work output per unit volume. The $W_{max}$ is calculated by

$$W_{max} = \frac{F_{max}\delta_{max}}{8wL(h_1 + h_2)}, \tag{6}$$

where $w$ and $h$ are the width and thickness of the actuator, respectively. Because the actuator prepared in this study was stimulated with a square wave voltage, the maximum work output per unit volume was divided by one-half of the period of time to calculate the maximum power output per unit volume. **Figure 11** allows for a comparison of the frequency and power output per unit volume, wherein the dashed lines link actuators that can produce equal $W_{max}$ in each cycle. In addition to the experimental results of this study, **Figure 11** gives some literature data for the previously reported CNT composite electrothermal actuators [8, 9], conventional electrothermal microactuators consisting of metals, ceramics and silicon [1, 5] and other kinds of bending actuators [32–34]. Chen et al. [8] have fabricated a 30-mm long aligned MWCNT-based polydimethylsiloxane (PDMS) composite electrothermal bimorph actuator (the thickness of the composite layer and PDMS layer was 20 and 750 μm, respectively) and achieved a bending displacement of 9.5 mm at a DC voltage of 40 V. Seo et al. [9] have fabricated a 33-mm long electrothermal actuator based on a PDMS slab sandwiched by upper and lower active layers of SWCNT/PDMS composites (the thickness of the composite layer and PDMS layer was about 0.5 and 500 μm, respectively). They reported a large bending displacement of 3.5 mm at a DC voltage of 60 V. Wang et al. [32] have prepared and evaluated a RAINBOW (reduced and internally biased oxide wafer) actuator consisting of a reduced electromechanically passive layer and an unreduced piezoelectric lead zirconate titanate (PZT) layer. Wang et al. [33] have investigated sulfonated poly(styrene-ran-ethylene) (SPSE) as a new ion-change membrane for use in ionomeric polymer-metal composite (IPMC) actuators. Cottinet et al. [34] have studied an IPMC actuator using a Nafion membrane and MWCNT buckypapers. The Young's moduli of the silicon, silicon oxide, silicon nitride, titanium tungsten, SPSE membrane, Nafion membrane, MWCNT buckypaper and PZT used in the above previous studies were estimated based on the literature values [1, 5, 32–34]. On the other hand, no information of the Young's moduli of the CNT composites and PDMS has been given in the literature [8, 9]. Thus, we estimated the Young's modulus of the composites using the rule of mixtures. We substituted $E_m = 0.85$ MPa and $E_f = 480$ GPa into Eq. (2) to estimate the Young's modulus of the aligned MWCNT/PDMS composite prepared by Chen et al. [8]. These values have been reported in the literature [26, 35]. In case of the actuators prepared by Seo et al. [9], the SWCNTs were randomly oriented in the composite layers. Therefore, we estimated the upper and lower limits

http://dx.doi.org/10.5772/62509

of the composite's Young's modulus using Eq. (1) and following Eq. (7), respectively [28], such that

$$E_c = \left[ \frac{V_f}{E_f} + \frac{(1 - V_f)}{E_m} \right]^{-1}. \tag{7}$$

The Young's moduli of PDMS (0.85 MPa) and SWCNTs (1200 GPa) have been reported in the literature [35, 36]. As shown in **Figure 11**, the actuator prepared in this study has higher values of power and work output per unit volume than that of the CNT composite actuators [8, 9] and IPMC actuators [33, 34]. This is mainly owing to the high Young's modulus of the actuator's constituents and the large bending displacement of the actuator. Although the actuators prepared by Chen et al. [8] and Seo et al. [9] can produce a large bending displacement, the thick pure PDMS layer may limit its force output. On the other hand, the actuator prepared in this study exhibited its large bending displacement and high force output because of the aligned MWCNT-reinforced epoxy composite and thin aluminum foil. The RAINBOW actuator [32] (7.0 × 1.02 × 40.0 $mm^3$ (length × width × thickness)) has a large power output per unit volume under the frequency of 250 Hz even though the bending displacement is in the range of 600 μm. This is mainly because the piezoelectric actuator provides the high force output at high operating frequency. On the other hand, the RAINBOW actuator may provide a power output per unit volume comparable to that of the IPMC actuators [33, 34] with a frequency between 0.05 and 2.5 Hz. In addition, its work output per unit volume is ≤ $10^{-4}$ mJ/$mm^3$, which is one order of magnitude lower than that of the actuator prepared in this study. The dimensions of the actuators prepared by Yang et al. [1] and Boutchich et al. [5] were 500–550 × 40–400 × 3.5 $\mu m^3$ (length × width × thickness). Even though the dimensions of the actuators prepared in this study are much larger than those of the actuators prepared by Yang et al. [1] and Boutchich et al. [5], it exhibits comparable or higher power and work output per unit volume under the frequency of 1.0 Hz. Furthermore, the applied voltage is 1–2 orders of magnitude smaller than that of the CNT composite electrothermal actuators [8, 9] and the RAINBOW actuator [32], which is almost identical to that of the IPMC actuators and electrothermal microactuators [1, 33, 34]. By employing microfabrication technology including photolithography, the dimensions of the electrothermal actuator can be decreased to the microscale with a length of hundreds of micrometers. Thus, the rate of heat dissipation as well as the frequency of the generated actuation can be greatly enhanced owing to the enhancement of the large surface-to-volume ratio. In addition, it is expected that the applied voltage may be potentially reduced because of the decrease in the electrical resistance of the actuator. In view of the significance of the Young's modulus and thermal expansion mismatch in these actuators, further studies should be carried out to miniaturize the CNT composite actuator. By developing CNT composite microactuators, a wide range of micro- and nanoscale applications can be envisioned where mechanical motion is needed at high displacement, high force and high speed, such as micromanipulation, optomechanical and electromechanical switches and mirrors, microfluidic valving and pumping, heat regulation and artificial muscles.

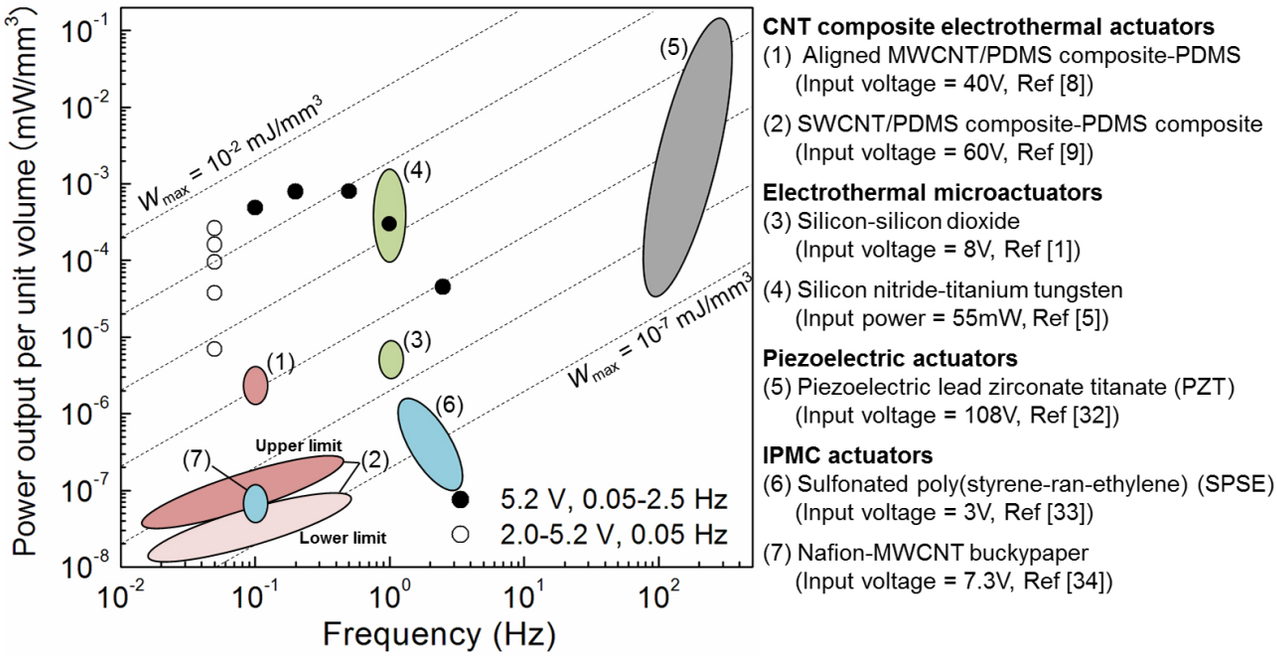


**Figure 11.** Actuator power output per unit volume as a function of frequency for this work (data points) and published reports (colored areas). The dashed lines link actuators that can produce equal maximum work output per unit volume in each cycle.

## 4. Conclusions

Combining an aligned MWCNT-reinforced polymer composite possessing a negative CTE in the MWCNT alignment direction with aluminum foil, we created a composite/aluminum bimorph that affords unique opportunities for the development of novel electrothermal actuators. The bending displacement and force output of the actuator, comprising an epoxy composite containing 27 vol.% MWCNTs and thin aluminum foil with a free length of 16 mm, reached 7.6 mm and 9.0 mN under a DC voltage of 5.2 V, respectively. Furthermore, the actuator fabricated in this study exhibited higher values of power and work output per unit volume than those of the actuators reported in previous studies with frequencies between 0.05 and 0.5 Hz. This was mainly owing to the high Young's moduli of both the composite and the aluminum layers as well as the huge mismatch of the CTEs in the composite/aluminum bimorph. The Young's modulus of the composites increased linearly with the increasing MWCNT volume fraction. The composite containing 27 vol.% MWCNTs produced the highest Young's modulus, with a value of 56.8 ± 3.9 GPa. We have also shown that the axial CTE of the MWCNTs was deduced to be $-1.1\times10^{-5}$ $K^{-1}$ from the CTE values measured on the aligned MWCNT/epoxy composites using the rule of mixtures, and the CTE of the composite containing 27 vol.% MWCNTs was $-0.7 \times 10^{-5}$ $K^{-1}$. In this study, we indicated contributions from three sources toward the increased bending displacement and force output in the actuator: (i) preparing the MWCNT/polymer composite to have a high Young's modulus and a negative CTE with the aid of an aligned MWCNT monolithic sheet; (ii) choosing materials with a high

Young's modulus and a large CTE as the second layer in the laminate; and (iii) designing the dimensional parameters of the actuator.

## Acknowledgements

The authors thank Prof. Y. Inoue and Prof. Y. Shimamura of Shizuoka University, Prof. T. Ogasawara of Tokyo University of Agriculture and Technology and Prof. T. Ono of Tohoku University for their useful guidance. The authors acknowledge Dr. T. Miyazaki of Technical Division, School of Engineering, Tohoku University, for technical assistance in the TEM analysis. The authors thank our colleagues, Mr. A. Nakamura and Mr. I. Tamaki of the Fracture and Reliability Research Institute (FRRI), Tohoku University, for their helpful discussions. This research was supported in part by the Japan Society for the Promotion of Science (JSPS) Core-to-Core Program. This research was partially supported by the Grant-in-Aid for JSPS 243582, the Grant-in-Aid for Young Scientists (A) 15H05502, the Grant-in-Aid for Research Activity Start-up 15H06025 and the Japan Science and Technology Agency through the Advanced Low Carbon Technology Research and Development Program (ALCA).

## Author details

Keiichi Shirasu*, Go Yamamoto and Toshiyuki Hashida

*Address all correspondence to: keiichi.shirasu@rift.mech.tohoku.ac.jp

Fracture and Reliability Research Institute, Tohoku University, Sendai, Japan

## References

[1] Yang JP, Deng XC, Chong TC . An electro-thermal bimorph-based microactuator for precise track-positioning of optical disk drives. Journal of Micromechanics and Microengineering. 2005;15:958–965.

[2] Zhu Y, Espinosa HD. An electromechanical material testing system for in situ electron microscopy and applications. Proceedings of the National Academy of Sciences of the United States of America. 2005;102:14503–14508.

[3] Lima MD, Li N, Jung de Andrade M, Fang S, Oh J, Spinks GM, Kozlov ME, Haines CS, Suh D, Foroughi J, Kim SJ, Chen Y, Ware T, Shin MK, Machado LD, Fonseca AF, Madden JDW, Voit WE, Galvão DS, Baughman RH. Electrically, chemically, and photonically powered torsional and tensile actuation of hybrid carbon nanotube yarn muscles. Science. 2012;338:928–932.

[4] Timoshenko S. Analysis of bi-metal thermostats. Journal of the Optical Society of America. 1925;11:233–255.

[5] Boutchich M, Mamtora TJ, McShane GJ, Haneef I, Moore DF, Williams JA. Force measurements on U-shaped electrothermal microactuators: applications to packaging. Proceedings of the Institution of Mechanical Engineers Part C-Journal of Mechanical Engineering Science. 2008;222:87–96.

[6] LeMieux MC, McConney ME, Lin YH, Singamaneni S, Jiang H, Bunning TJ, Tsukruk VV. Polymeric nanolayers as actuators for ultrasensitive thermal bimorphs. Nano Letters. 2006;6:730–734.

[7] Liu K, Cheng C, Cheng Z, Wang K, Ramesh R, Wu J. Giant-amplitude, high-work density microactuators with phase transition activated nanolayer bimorphs. Nano Letters. 2012;12:6302–6308.

[8] Chen L, Liu C, Liu K, Meng C, Hu C, Wang J, Fan S. High-performance, low-voltage, and easy-operable bending actuator based on aligned carbon nanotube/polymer composites. ACS Nano. 2011;5:1588–1593.

[9] Seo DK, Kang TJ, Kim DW, Kim YH. Twistable and bendable actuator: a CNT/polymer sandwich structure driven by thermal gradient. Nanotechnology. 2012;23:075501 (7pp).

[10] Zeng Z, Jin H, Zhang L, Zhang H, Chen Z, Gao F, Zhang Z. Low-voltage and high-performance electrothermal actuator based on multi-walled carbon nanotube/polymer composites. Carbon. 2015;84:327–334.

[11] Ruoff RS, Lorents DC. Mechanical and thermal properties of carbon nanotubes. Carbon. 1995;33:925–930.

[12] Ebbesen TW, Lezec HJ, Hiura H, Bennett JW, Ghaemi HF, Thio T. Electrical conductivity of individual carbon nanotubes. Nature. 1996;382:54–56.

[13] Peng B, Locascio M, Zapol P, Li S, Mielke SL, Schatz GC, Espinosa HD. Measurements of near-ultimate strength for multiwalled carbon nanotubes and irradiation-induced crosslinking improvements. Nature Nanotechnology. 2008;3:626–631.

[14] Schelling PK, Keblinski P. Thermal expansion of carbon structures. Physical Review B. 2003;68:035425 (7pp).

[15] Kwon YK, Berber S, Tománek D. Thermal contraction of carbon fullerenes and nanotubes. Physical Review Letters. 2004;92:015901 (4pp).

[16] Jiang H, Liu B, Huang Y, Hwang KC. Thermal expansion of single wall carbon nanotubes. Journal of Engineering Materials and Technology. 2004;126:265–270.

[17] Alamusi, Hu N, Jia B, Arai M, Yan C, Li J, Liu Y, Atobe S, Fukunaga H. Prediction of thermal expansion properties of carbon nanotubes using molecular dynamics simulations. Computational Materials Science. 2012;54:249–254.

[18] Zhang M, Fang S, Zakhidov AA, Lee SB, Aliev AE, Williams CD, Atkinson KR, Baughman RH. Strong, transparent, multifunctional, carbon nanotube sheets. Science. 2005;309:1215-1219.

[19] Cheng Q, Wang J, Jiang K, Li Q, Fan S. Fabrication and properties of aligned multi-walled carbon nanotube-reinforced epoxy composites. Journal of Materials Research. 2008;23:2975–2983.

[20] Bradford PD, Wang X, Zhao H, Maria JP, Jia Q, Zhu YT. A novel approach to fabricate high volume fraction nanocomposites with long aligned carbon nanotubes. Composites Science and Technology. 2010;70:1980–1985.

[21] Ogasawara T, Moon SY, Inoue Y, Shimamura Y. Mechanical properties of aligned multi-walled carbon nanotube/epoxy composites processed using a hot-melt prepreg method. Composites Science and Technology. 2011;71:1826–1833.

[22] Liu W, Zhang X, Xu G, Bradford PD, Wang X, Zhao H, Zhang Y, Jia Q, Yuan FG, Li Q, Qiu Y, Zhu Y. Producing superior composites by winding carbon nanotubes onto a mandrel under a poly(vinyl alcohol) spray. Carbon. 2011;49:4786–4791.

[23] Wang X, Yong ZZ, Li QW, Bradford PD, Liu W, Tucker DS, Cai W, Wang H, Yuan FG, Zhu YT. Ultrastrong, stiff and multifunctional carbon nanotube composites. Materials Research Letters. 2013;1:19–25.

[24] Inoue Y, Kakihata K, Hirono Y, Horie T, Ishida A, Mimura H. One-step grown aligned bulk carbon nanotubes by chloride mediated chemical vapor deposition. Applied Physics Letters. 2008;92:213113 (3pp).

[25] Yamamoto G, Suk JW, An J, Piner RD, Hashida T, Takagi T, Ruoff RD. The influence of nanoscale defects on the fracture of multi-walled carbon nanotubes under tensile loading. Diamond and Related Materials. 2010;19:748–751.

[26] Yamamoto G, Shirasu K, Nozaka Y, Sato Y, Takagi T, Hashida T. Structure-property relationships in thermally-annealed multi-walled carbon nanotubes. Carbon. 2014;66:219–226.

[27] Spitalsky Z, Tasis D, Papagelis K, Galiotis C. Carbon nanotube–polymer composites: Chemistry, processing, mechanical and electrical properties. Progress in Polymer Science. 2010;35:357–401.

[28] Hull D, Cryne TW. An Introduction to Composite Materials. 2nd ed. Cambridge: Cambridge University Press; 1996.

[29] Raravikar NR, Keblinski P, Rao AM, Dresselhaus MS, Schadler LS, Ajayan PM. Temperature dependence of radial breathing mode Raman frequency of single-walled carbon nanotubes. Physical Review B. 2002;66:235424 (9pp).

[30] Li C, Chou TW. Axial and radial thermal expansions of single-walled carbon nanotubes. Physical Review B. 2005;71:235414 (6pp).

[31] Ashcroft NW, Mermin ND. Solid State Physics. New York: Holt, Reinhart, and Winston; 1976.

[32] Wang QM, Zhang Q, Xu B, Liu R, Cross LE. Nonlinear piezoelectric behavior of ceramic bending mode actuators under strong electric fields. Journal of Applied Physics. 1999;86:3352–3360.

[33] Wang XL, Oh IK, Cheng TH. Electro-active polymer actuators employing sulfonated poly(styrene-ran-ethylene) as ionic membranes. Polymer International. 2010;59:305–312.

[34] Cottinet PJ, Souders C, Labrador D, Porter S, Liang Z, Wang B, Zhang C. Nonlinear strain–electric field relationship of carbon nanotube buckypaper/Nafion actuators. Sensors and Actuators A: Physical. 2011;170:164–171.

[35] Chen LZ, Liu CH, Hu CH, Fan SS. Electrothermal actuation based on carbon nanotube network in silicone elastomer. Applied Physics Letters. 2008;92:263104 (3pp).

[36] Tombler TW, Zhou C, Alexseyev L, Kong J, Dai H, Liu L, Jayanthi CS, Tang M, Wu SY. Reversible electromechanical characteristics of carbon nanotubes under local-probe manipulation. Nature. 2000;405:769–772.